DOI: 10.1002/ejoc.200701125

The Tetracyanoquinodimethane Motif in Overcrowded Bistricyclic Aromatic Enes: Avoiding Thermochromism

Sergey Pogodin,[a] Michal Rachel Suissa,[a][‡] Amalia Levy,[a] Shmuel Cohen,[b] and Israel Agranat*[a]

Keywords: Thermochromism / Strained molecules / Conformation analysis / Density functional calculations / X-ray crystal structure

The overcrowded bistricyclic aromatic enes (BAEs) [10-[10-(dicyanomethylene)-9(10*H*)-anthracenylidene]-9(10*H*)-anthracenylidene]propanedinitrile (**7**) and [10-[10-oxo-9(10*H*)-anthracenylidene]-9(10*H*)-anthracenylidene)]propanedinitrile (**8**) were synthesized by a condensation of bianthrone (**2**) with malononitrile in the presence of $TiCl_4$ and pyridine. The crystal and molecular structure of **7** were determined. It crystallizes in two polymorphic forms, belonging to the space groups $P2_1/c$ and $P2_1/n$. DFT calculations of **7** and **8** show that the overcrowding due to introducing dicyanomethylene substituents to 10 and 10′ positions is more pronounced in the twisted conformations, decreasing their stabilities. The enthalpy differences between the *anti*-folded and the lowest lying twisted conformations in BAEs **7** and **8** are 61.3 and 42.3 kJ/mol, respectively. In accordance with theory, BAEs **7** and **8** do not exhibit thermochromic behavior.

Introduction

The bistricyclic aromatic enes (BAEs, Figure 1) have fascinated chemists since the red 9-(9′*H*-fluoren-9′-ylidene)-9*H*-fluorene (bifluorenylidene, **1**) was synthesized in 1875.[1] They are attractive substrates for the study of the conformational behavior and dynamic stereochemistry of overcrowded polycyclic aromatic enes and for the interplay of strain and delocalization effects.[2] BAEs are classified as *homomerous* (Figure 1, X = Y) and *heteromerous* bistricyclic aromatic enes (Figure 1, X ≠ Y). The phenomenon of thermochromism,[3] i.e. reversible change of color with change of temperature, was discovered in overcrowded BAEs in 1909.[4] Yellow solutions of 10-[10′-oxo-9′(10′*H*)-anthracenylidene]-9(10*H*)-anthracenone (bianthrone, **2**) reversibly turn dark green upon heating.[4] The color change may also be triggered by pressure (piezochromism)[5] or by UV irradiation (photochromism).[3e,6] Thermochromic and photochromic BAEs serve as candidates for chiroptical molecular switches and molecular motors.[7] Derivatives of **2** are topologically related to hypericin, widespread in St. Johns Wort, an important remedy against depression.[8] A tetradehydrodianthracene unit, also topologically related to **2**, is a beltlike pyramidalized component of the first Möbius annulene.[9]

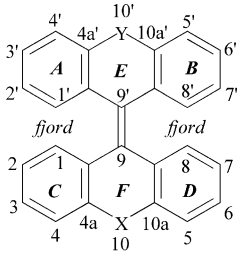

Figure 1. Bistricyclic aromatic enes.

Thermochromism in BAEs has been attributed to an unimolecular equilibrium between two distinct and interconvertible conformers: a colorless or yellow room-temperature form **A** and a deep-colored high-temperature form **B**, with 4–30 kJ/mol of the enthalpy differences between them.[10]

$$\mathbf{A} \underset{}{\overset{kT}{\rightleftharpoons}} \mathbf{B}$$

While form **A** absorbs in the UV region or close to it, the thermochromic form **B** has a new absorption band at $\lambda \approx 600$–700 nm. The thermochromic, photochromic, and piezochromic **B** forms are considered to be identical.[6c,10c,10f,11] Recently the controversial nature of the

[a] Department of Organic Chemistry, The Hebrew University of Jerusalem,
Jerusalem 91904, Israel
Fax: +972-2-6511907
E-mail: isria@vms.huji.ac.il
[b] Department of Inorganic and Analytical Chemistry, The Hebrew University of Jerusalem,
Jerusalem 91904, Israel
[‡] Present address: Oslo University College, Faculty of Health Sciences/Pharmacy,
Oslo, Norway
Supporting information for this article is available on the WWW under http://www.eurjoc.org or from the author.

thermochromic phenomenon in BAEs has been resolved: the deeply colored thermochromic form **B** was identified as the twisted conformation.[3f] The high twist of the central double bond reduces the π-overlap and causes a substantial red shift. The yellow or colorless room-temperature form **A** was identified as *anti*-folded conformations.

Three types of conformational behavior have been distinguished in BAEs.[12] Type 1 BAEs can show thermochromism if an energy difference between the global minimum *anti*-folded **a** or unevenly *anti*-folded **au** conformation (corresponding to the room temperature form **A**) and the local minimum twisted conformation **t** (corresponding to the thermochromic form **B**) is sufficiently small to allow thermal population of **t**, i.e. less than 30 kJ/mol, based on experimental data and DFT calculations.[12] Examples of Type 1 BAEs are bianthrone (**2**) and 9,9′-bi-9*H*-xanthen-9-ylidene (dixanthylene, **3**). Type 2 BAEs also adopt *anti*-folded conformations as global minima, but their twisted conformations cannot be populated in thermal equilibrium, and their *syn*-folded conformations **s** are usually more stable than the twisted conformations. Therefore, Type 2 BAEs, for example, 9,9-bi(9*H*-thioxanthen-9-ylidene) (**4**), do not exhibit thermochromic behavior.[13] Type 3 BAEs adopt twisted conformations as their global minima. Their thermochromic forms dominate in the equilibrium at all temperatures and are responsible for the deep color of these compounds. 9-(9′*H*-fluoren-9′-ylidene)-9*H*-xanthene (fluorenylidene-xanthene, **5**), which has a deep purple color in solution, belongs to Type 3. The folded conformations of Type 3 BAEs, although usually higher in energy than the twisted conformations, may be populated in equilibrium, but their color is masked by the deeply colored twisted conformations. Packing effects may favor the folded conformations.[14]

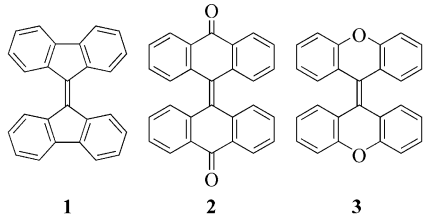

1 **2** **3**

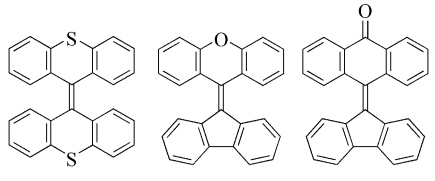

4 **5** **6**

Affecting the equilibrium between twisted and folded conformations of a BAE would result in changes of its conformational space and physical properties. We became interested in the control of the relative stabilities of twisted and folded conformations by various structural modifications to alter their thermochromic properties. Very recently we have reported thermochromism at room temperature in Type 3 BAEs in the series of fluorenylidene-anthrone (**6**) and its 1,8-diazasubstituted derivatives due to closely populated twisted and folded conformations.[15] The nature of the bridges X and Y of BAEs (Figure 1) has been shown to exert a profound effect on the relative stabilities of the conformations of BAEs. Such an effect would result in changes of their physical properties, including thermochromism. We have decided to explore the thermochromic behavior of BAEs with dicyanomethylene bridges; X, Y = $C=C(CN)_2$. We report here the synthesis of [10-[10-(dicyanomethylene)-9(10*H*)-anthracenylidene]-9(10*H*)-anthracenylidene]propanedinitrile (**7**) and [10-[10-oxo-9(10*H*)-anthracenylidene]-9(10*H*)-anthracenylidene)]propanedinitrile (**8**), the crystal and molecular structure of **7**, and the conformational spaces of **7** and **8** as determined by the DFT calculations. We note that neither **7** nor **8** are proved to be thermochromic.

Results and Discussion

Synthesis

The syntheses of **7** and **8** were accomplished by a direct condensation of bianthrone (**2**) with excess malononitrile in boiling chloroform, in the presence of $TiCl_4$ and pyridine, using the procedure of Hünig et al. (Scheme 1).[16] BAEs **7** and **8** were separated by trituration in boiling chloroform. Orange single crystals of **7**, mp. 466 °C, were obtained by sublimation. The starting material **2** was removed from crude **8** by column chromatography, and **8** was then purified by sublimation to give yellow-orange powder, m.p. 325 °C. The yields of **7** and **8** were 14% and 7%, respectively. The synthesis of **7**, mp. >300 °C, has previously been reported.[17] The structures of **7** and **8** were first established by elemental analysis, infrared ($\tilde{\nu}_{max}$ = = 2219.5 (CN, **7**), 2222.3 (CN, **8**) and 1671.8 (CO, **8**) cm^{-1}) and mass spectroscopy (molecular ions *m*/*z* (%): 480 (100) [$C_{34}H_{16}N_4^+$, **7**], 432 (100) [$C_{31}H_{16}N_2O^+$, **8**]), as well as by ^1H and ^{13}C NMR spectroscopy. The following characteristic chemical shifts have been observed. The *fjord* regions' protons of **7** (H^1, $H^{1'}$, H^8, H^8) appeared at δ = 7.24 ppm ([D_6]DMSO). The hydrogen atoms *peri* to the dicyanomethylene groups of **7**

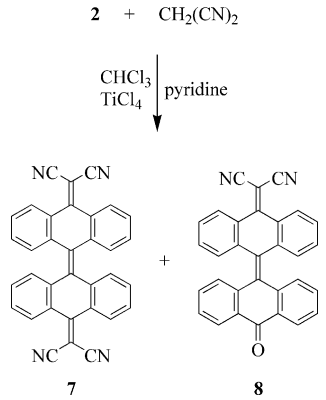

7 **8**

Scheme 1. The synthesis of BAEs **7** and **8**, dicyanomethylene derivatives of bianthrone (**2**).

(H^4, $H^{4'}$, H^5, $H^{5'}$) appeared at δ = 8.12 ppm ($C_2D_2Cl_4$). The carbons of the dicyanomethylene groups of **7** appeared at 99.7 (C^{11}, $C^{11'}$), 113.9 (C^{12}, $C^{12'}$, C^{13}, $C^{13'}$) and 164.1 (C^{10}, $C^{10'}$) ppm. For comparison, in tertacyanoquinoanthradimethane (**9**) the corresponding carbon chemical shifts are 83.1, 112.9 and 160.0 ppm, respectively.[18] The *fjord* regions' protons of **8** (H^1, $H^{1'}$, H^8, H^8) appeared at δ = 7.09 and 7.18 ppm ($CDCl_3$). The hydrogens *peri* to the carbonyl (H^4, H^5) and the dicyanomethylene groups of **8** ($H^{4'}$, $H^{5'}$) appeared at δ = 8.06 and 8.13 ppm ($C_2D_2Cl_4$). The carbons of the dicyanomethylene groups of **8** appeared at 79.2 ($C^{11'}$), 114.2 ($C^{12'}$, $C^{13'}$) and 164.9 ($C^{10'}$) ppm. The carbonyl carbon of **8** (C^{10}) appeared at δ = 186.3 ppm. The ^{1}H NMR chemical shifts of the *fjord* region hydrogens of **7** and **8** indicate that these BAEs adopt *anti*-folded conformations in solution, similarly to bianthrone (**2**).[19]

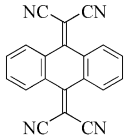

9

BAEs **7** and **8** are orange and yellow, respectively, in the solid state. Their colors do not change in solution, indicating the absence of readily populated twisted conformations. Heating of solid **7** and **8** up to temperature of 300° also did not lead to any color change. Thus, **7** and **8** does not show thermochromic behaviour.

Molecular and Crystal Structure

The crystal data of **7** are given in Table 3 (a preliminary description of the crystal structure of **7** has been reported in The International Symposium on "Molecular Structure: Chemical Reactivity and Biological Activity", Beijing, People's Republic of China, 15–21 September 1986; see ref.[2a]).[20] Table 1 shows selected structural parameters of **7** derived from the crystal structures and from DFT calculations (vide infra). Structural parameters defined as follows: pure ethylenic twists[2c] ω_1 and ω_2 around C^9=$C^{9'}$ and C^{10}=C^{11} are the average values of the torsion angles C^{9a}–C^9–$C^{9'}$–$C^{9a'}$ and C^{8a}–C^9–$C^{9'}$–$C^{8a'}$ (ω_1) and C^{4a}–C^{10}–C^{11}–C^{12} and C^{10a}–C^{10}–C^{11}–C^{13} (ω_2), respectively; *fjord* twist (ϕ) is the average values of the torsion angles C^1–C^9–$C^{9'}$–$C^{1'}$ and C^8–C^9–$C^{9'}$–$C^{8'}$; fold[2c] of the tricyclic moiety (*A*–*B* or *C*–*D*, see Figure 1) is defined as the dihedral angle between the least-square planes of the atoms of the benzene rings of each tricyclic moiety; bistricyclic dihedral (AEB–CFD, see Figure 1) is defined as the dihedral angle between the least-square planes of all the untagged and all the tagged atoms of the tricyclic moieties; pyramidalization angles[2c] $\chi(C^9)$, $\chi(C^{10})$ and $\chi(C^{11})$ are defined as the improper torsion angles C^{9a}–C^9–$C^{9'}$–C^{8a}, C^{4a}–C^{10}–C^{11}–C^{10a} and C^{12}–C^{11}–C^{10}–C^{13}, respectively, minus 180°. The overall conformations of the bistricyclic aromatic enes are characterized by the pure twist of the central C^9=$C^{9'}$ bond and by the folding dihedral of the tricyclic moieties.[2b]

Table 1. Conformations and selected structural parameters of X-ray determined structures and calculated minima of **7** and **8** (at B3LYP/6-311G(d,p)).

		ω_1	ω_2 ω_2'	ϕ ϕ'	A–B C–D	AEB– CFD	$\chi(C^9)$ $\chi(C^{9'})$	$\chi(C^{10})$ $\chi(C^{10'})$	$\chi(C^{11})$ $\chi(C^{11'})$	C^9=$C^{9'}$	C^{10}=C^{11} $C^{10'}$=$C^{11'}$	C^1···$C^{1'}$ C^8···$C^{8'}$	H^1···$C^{1'}$ $H^{1'}$···C^1 H^8···$C^{8'}$ $H^{8'}$···C^8	H^4···$C^{12'}$ $H^{4'}$···C^{12} H^5···$C^{13'}$ $H^{5'}$···C^{13}	C^4···$C^{12'}$ $C^{4'}$···C^{12} C^5···$C^{13'}$ $C^{5'}$···C^{13}
		deg	deg	deg	deg	deg	deg	deg	deg	pm	pm	pm	pm	pm	pm
7–a	C_{2h}	0.0	0.0	39.4 –39.4	50.5	0.0	–1.8	1.1	–4.2	136.1	137.1	312.2	297.7	256.8	302.3
LT-7[a]	–	–1.1	–4.2 4.2	–39.2 37.5	47.2 47.9	3.3	0.1 2.1	–1.4 –1.3	7.2 7.1	135.3	136.5 136.1	301.3 302.6	280.9 291.7 286.6 281.4	254.3 261.3 259.8 252.9	297.1 302.3 301.1 297.8
RT-7[b]	–	0.0	–4.4	–38.2	47.7	0.0	1.4	–1.7	6.5	135.5	136.3	302.4	287.0 291.2	251.2 259.4	298.5 302.7
7–s	C_{2v}	0.0	0.0	0.0	52.9	71.5	–16.8 16.8	–0.5 0.5	–2.2 2.2	136.2	136.9	317.3	276.1	254.1	302.0
7–ta	C_2	–57.7	1.6	–76.3 –55.8	20.0	62.0	–1.4	–6.5	7.2	143.4	138.9	302.7 341.4	256.2 325.8	236.8 240.1	285.9 288.6
7–ts	C_2	51.7	–0.5	59.9	30.9	65.3	2.0 –2.0	4.3 –4.3	–5.9 5.9	141.5	138.1	314.8	255.2 298.2	241.4 247.7	290.2 293.8
8–au	C_s	0.0	– 0.0	–37.7 37.7	39.2 52.6	0.9	4.5 1.3	8.3 –0.5	– 3.9	136.3	– 137.1	306.5	293.1 292.6	– 257.7	– 303.3
8–su	C_s	0.0	– 0.0	2.1 –2.1	39.1 55.8	68.6	18.1 –20.3	8.8 –0.5	– –2.5	136.4	– 136.8	313.2	268.5 282.7	– 257.8	– 304.4
8–tf	C_1	–55.3	– 1.1	–59.2 –68.4	7.8 24.5	62.3	–1.2 2.6	1.6 5.4	– –6.8	142.4	– 138.6	307.5 324.2	277.3 259.2 290.4 309.2	– 238.5 – 243.1	– 287.7 – 290.6

[a] X-ray structure, at 173 K. [b] X-ray structure, at 295 K.

Figure 2 gives ORTEP diagram of one molecule of **7**, as determined by the low-temperature X-ray analysis (anisotropic displacement parameters are drawn at the 50% probability level). BAE **7** crystallizes in two polymorphic form. At room temperature (**RT-7**, 295 K) **7** crystallizes in the monoclinic space group $P2_1/c$ with two molecules in the unit cell, in which the central double bond $C^9=C^{9'}$ of each molecule of **7** lies on the inversion center. This molecular structure exhibit stacking of aromatic rings of **7**. Rings *A* (Figure 1) of two neighboring molecules of **7** are rotated by 180° one relative to another and form columns with a distance of 400 pm between their centers. Rings *C* are arranged analogously. Rings *B* (in analogously, ring *D*) lie on the planes which are parallel to the *xy* plane, but are shifted one relative to another and do not form stacks. Their centers are separated by 664 pm. At low temperature (**LT-7**, 173 K) **7** crystallizes in the monoclinic space group $P2_1/n$ with four molecules in the asymmetric unit. In this form each molecule of **7** is chiral and the unit cell consist of two pairs of enantiomers. Similarly to the room temperature crystal structure, rings *A* of the neighboring molecules of **7** form stacks in which the rings are rotated by 180° one relative to another and separated by 397 pm. Analogously, rings *C* are arranged in columns which are parallel to these formed by rings *A* and separated by 403 pm. The briefly described literature crystal structure of **7**[17] indicates a third polymorphic form, having space group $P2_1/a$ with cell dimensions a = 8.912 Å, b = 22.390 Å, c = 8.4318 Å, γ = 107.66°, and Z = 2.

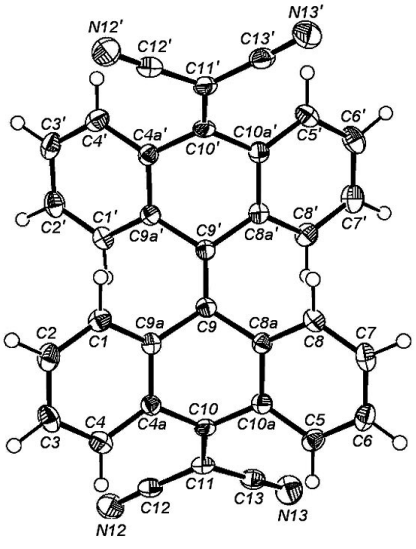

Figure 2. ORTEP drawing of the low-temperature molecular structure of **7**.

Both **RT-7** and **LT-7** molcular structures indicate that the molecules of BAE **7** adopt an *anti*-folded conformation, which is characterized by small pure twist angles (ω_1 = 0.0° (**RT-7**) and –0.8° (**LT-7**), ω_2 = ±4.4° (**RT-7**) and ±4.2 (**LT-7**)) and significant folding (*A*–*B* 47.7° (**RT-7**) and 47.9° and 47.2° (**LT-7**)). There is 6–7° pyramidalization of C^9 and $C^{9'}$. The central six membered rings of **7** adopt boat conformations to release the steric repulsion between the dicyanomethylene groups and the *peri* hydrogen atoms. The dihedral angles between the C^{4a}–C^{10}–C^{10a} and C^{8a}–C^9–C^{9a} planes are 67.8° (**RT-7**) and 65.8° and 68.5° (**LT-7**). Nevertheless, the degree of overcrowding in the *fjord* regions and around the dicyanomethylene groups of **7**, as reflected in the intramolecular distances $C^1\cdots C^{1'}$, $C^4\cdots C^{12}$ ($C^{4'}\cdots C^{12'}$), and $H^4\cdots C^{12}$ ($H^{4'}\cdots C^{12'}$) are still significant: 301–302, 297–302, and 251–261 ppm, respectively. These distances correspond to 12, 12–13, and 9–12% of penetration, based on the van der Waals radii of carbon (δ = 171 ppm) and hydrogen (δ = 115 ppm).[21]

DFT Study

DFT methods are capable of generating a variety of isolated molecular properties quite accurately, especially via the hybrid functionals, and in a cost-effective way.[22] Recently, the B3LYP hybrid functional was successfully employed to treat overcrowded BAEs.[15,23] BAEs **7** and **8** were subjected to a systematic computational DFT study of their conformational spaces and of the relative stabilities of their *anti*-folded and twisted conformations. The relative energies of these BAEs are presented in Table 2. Selected geometrical parameters of the BAEs under study are presented in Table 1. Figure 3 and Figure 4 show the calculated minima and transition state conformations of **7**. The designators of conformations are defined in accordance with the literature.[2c] The following analysis is based on the DFT B3LYP/6-311G(d,p) enthalpies ΔH_{298}. BAE **7** adopts the *anti*-folded conformation C_{2h}–**7**–**a** (*A*–*B* 50.5°) as the global minimum. Its *syn*-folded conformation C_{2v}–**7**–**s** is less stable than C_{2h}–**7**–**a** by 46.4 kJ/mol and is characterized by the larger folding angle (*A*–*B* 52.9°) and significantly larger pyramidalization at C^9 (χ = 16.8° vs. 1.8° in C_{2h}–**7**–**a**). The central six membered rings of **7** adopt boat conformations, with the dihedral angles between the C^{4a}–C^{10}–C^{10a} and C^{8a}–C^9–C^{9a} planes of 70.0° (C_{2h}–**7**–**a**) and 74.6° (C_{2v}–**7**–**s**). Both folded conformations are moderately overcrowded in the regions around $C^{10}=C^{11}$ and $C^{10'}=C^{11'}$: the $C^4\cdots C^{12}$ and $C^5\cdots C^{13}$ non-bonding distances are ca. 302 pm (12% penetration), while $H^4\cdots C^{12}$ and $H^5\cdots C^{13}$ distances are 257 pm (10% penetration) in C_{2v}–**7**–**a** and 254 pm (11% penetration) in C_{2v}–**7**–**s**. The *fjord* regions around the central double bond are the secondary source of overcrowding in C_{2v}–**7**–**a** and C_{2v}–**7**–**s**: the $C^1\cdots C^{1'}$ and $C^8\cdots C^{8'}$ distances are 312 and 317 pm (9 and 7% penetration), respectively, while $H^1\cdots H^{1'}$ and $H^8\cdots H^{8'}$ distance in C_{2v}–**7**–**s** is 203 pm (12% penetration). Both room temperature and low temperature molecular structures of **7** as determined by X-ray crystallography correspond to the DFT-calculated *anti*-folded C_{2h}–**7**–**a** conformation, but the calculated structure is in better agreement with the **RT-7** structure due to the higher point symmetry of the latter (C_i). The only notable difference between **RT-7** X-ray molecular structure and the calculated structure is the longer $C^1\cdots C^{1'}$ distance in the latter, 312 vs. 302 pm.

The third folded conformation [C_s–**7**–**f**] resembles the *syn*-folded C_{2v}–**7**–**s** conformation, but demonstrates an un-

Table 2. The DFT relative energies [kJ/mol] and characteristic structural parameters [°] of **7** and **8**.

		B3LYP/6-31G(d)							B3LYP/6-311G(d,p)						
		[a]	ΔE_{Tot}	ΔH_{298}	ΔG_{298}	ω_1	ω_2	A–B C–D	[a]	ΔE_{Tot}	ΔH_{298}	ΔG_{298}	ω_1	ω_2	A–B C–D
7–a	C_{2h}	M	0.0	0.0	0.0	0.0	0.0	49.9	M	0.0	0.0	0.0	0.0	0.0	50.5
7–s	C_{2v}	M	48.0	47.4	41.5	0.0	0.0	52.0	M	46.9	46.4	40.4	0.0	0.0	52.9
7–(*MPM*)–**ts**	C_2	M	57.8	57.0	55.7	52.8	–0.5	28.7	M	62.2	61.3	60.1	51.7	–0.5	30.9
7–(*PMP*)–**ta**	C_2	M	67.4	66.5	65.8	–57.6	1.5	19.3	M	73.3	72.4	71.6	–57.7	1.6	20.0
7–(*PMP*)–**tf**	C_1	TS	80.8	77.5	81.6	–59.7	26.4	8.4	TS	87.3	79.1	83.0	–60.0	27.1	4.7
							1.1	22.3						1.2	22.3
7–(*PMP*)–**t**	D_2	SP2	96.7	90.7	104.6	–64.0	27.0	6.2	SP2	104.2	93.2	106.6	–64.3	27.4	6.4
7–(*PMM*)–**t**	C_2	SP2	100.1	94.0	106.4	–63.1	–24.4	5.9	SP2	107.6	96.5	108.5	–63.5	–24.5	6.3
							–27.4	14.5						27.6	15.1
7–(*MMM*)–**t**	D_2	SP2	103.6	97.5	111.8	–62.5	–24.7	14.5	SP2	111.2	100.0	114.1	–62.6	–24.7	15.1
7–f	C_s	SP2	122.8	117.4	128.9	0.0	0.0	17.4	TS	121.8	114.3	111.8	0.0	0.0	17.7
								73.6							74.1
8–au	C_s	M	0.0	0.0	0.0	0.0	0.0	39.1	M	0.0	0.0	0.0	0.0	0.0	39.2
								52.0							52.6
8–(*MP*)–**tf**	C_1	M	37.7	37.1	36.0	–55.4	–	7.1	M	42.9	42.3	40.8	–55.3	–	7.8
							1.1	23.6						1.1	24.5
8–su	C_s	M	44.0	43.4	38.1	0.0	0.0	38.6	M	43.0	42.5	37.7	0.0	0.0	39.1
								54.9							55.8
8–(*MP*)–**t**	C_2	TS	55.7	52.5	59.5	–59.2	–	3.5	TS	62.1	58.7	65.2	–59.4	–	4.0
							27.1	5.0						27.7	5.1
8–(*PP*)–**ft**	C_1	TS	91.1	88.6	91.1	14.6	–	10.2	TS	90.4	88.2	90.9	13.1	–	10.2
							1.2	69.4						1.1	70.7
8–f	C_s	SP2	91.8	86.9	98.3	0.0	–	3.1	SP2	91.1	86.3	97.7	0.0	–	3.4
							0.0	74.1						0.0	74.7

[a] M = minimum, TS = transition state, SP2 = 2nd order saddle point.

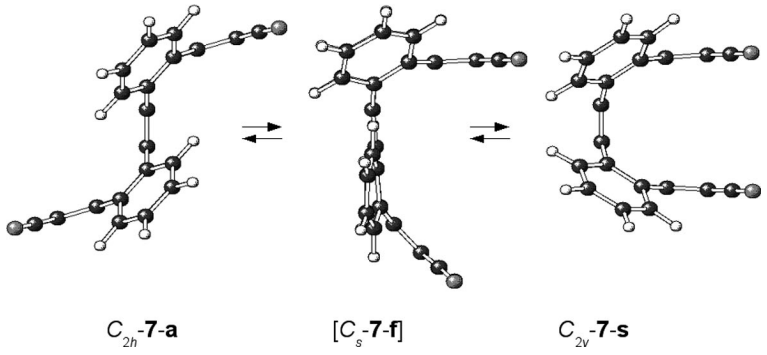

Figure 3. The B3LYP/6-311(d,p)-calculated folded conformations of **7** and the transition state for their interconversion.

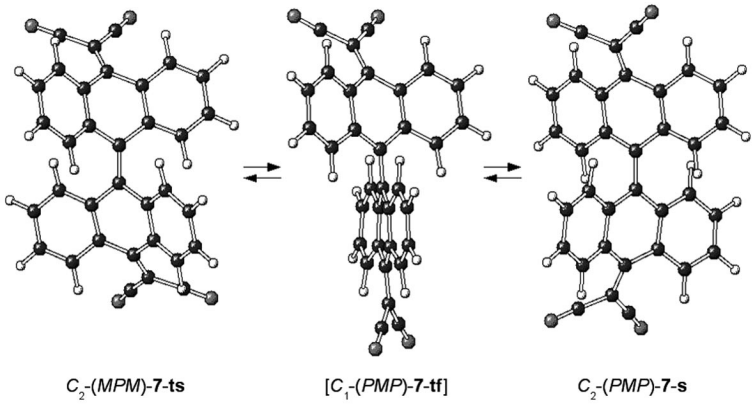

Figure 4. The B3LYP/6-311(d,p)-calculated twisted conformations of **7** and the transition state for their interconversion.

equal folding (*A–B* 17.7°, *C–D* 74.1°) of its bistricyclic moieties. It serves as a transition state for the interconversion of the folded C_{2h}–**7**–**a** and C_{2v}–**7**–**s** conformations, with the enthalpy barriers of 114.3 and 67.9 kJ/mol, respectively.

These high barriers are due to the short $H^1\cdots C^{1'}$ and $H^8\cdots C^{8'}$ distances in the *fjord* region (216 pm).

The lowest lying twisted conformation C_2–(*MPM*)–**7**–**ts** is 61.3 kJ/mol less stable than C_{2v}–**7**–**a**. It is characterized by both twisting of the molecule around $C^9{=}C^{9'}$ (ω_1 = 51.7°) and $C^{10}{=}C^{11}$ (ω_2 = –0.5°) and *syn*-folding of its bistricyclic moieties (*A*–*B* 30.9°). It is more overcrowded than the folded conformations. The contact distances $C^4\cdots C^{12}$, $C^5\cdots C^{13}$, $H^4\cdots C^{12}$, and $H^5\cdots C^{13}$ are 290, 294, 241, and 248 pm (13–16% penetration). The twisted-*anti*-folded conformation C_2–(*PMP*)–**7**–**ta** (ω_1 = –57.7°, ω_2 = 1.6°, *A*–*B* 20.0°) is 72.4 kJ/mol less stable than C_{2v}–**7**–**a** and 11.0 kJ/mol less stable than C_2–(*MPM*)–**7**–**ts**. It is more overcrowded than C_2–(*MPM*)–**7**–**ts**, with the contact distances $C^4\cdots C^{12}$, $C^5\cdots C^{13}$, $H^4\cdots C^{12}$, and $H^5\cdots C^{13}$ of 286, 289, 237, and 240 pm (16–17% penetration). Another twisted-folded conformation [C_1–(*PMP*)–**7**–**tf**] is less stable than C_{2h}–**7**–**a** by 79.1 kJ/mol. It is characterised by a combination of a twisting mode dominating one bistricyclic moiety of the molecule (ω_1 = –60.0°, ω_2 = 27.1°, *A*–*B* 4.7°) and a folding mode dominating the other bistricyclic moiety (ω_2 = 1.2°, *A*–*B* 22.3°). This conformation serves as a transition state for the interconversion of the twisted C_2–(*MPM*)–**7**–**ts** and C_2–(*PMP*)–**7**–**ta** with the enthalpy barriers of 17.8 and 6.8 kJ/mol, respectively. Three additional twisted conformations D_2–(*PMP*)–**7**–**t**, C_2–(*PMM*)–**7**–**t**, and D_2–(*MMM*)–**7**–**t** lie 93.2, 96.5, and 100.0 kJ/mol, respectively, higher than C_{2v}–**7**–**a**. They are 2nd order saddle points and are severely overcrowded, having the $H^4\cdots C^{12}$ ($H^{4'}\cdots C^{12'}$) distances of 216–217 pm (24–25% penetration). The high enthalpy differences between the *anti*-folded global minimum and twisted **ts** (61.3 kJ/mol) and **ta** (72.4 kJ/mol) local minima indicate that **7** belong to Type 2 BAEs. Including of the entropy corrections lowers the above values by only ca. 1 kJ/mol. Thus, the twisted conformations of **7** are not thermally populated, excluding any thermochromic properties of **7**.

BAE **8** adopts the unequally *anti*-folded conformation C_s–**8**–**au** (*A*–*B* 39.2°, *C*–*D* 52.6°) as the global minimum. Its unequally *syn*-folded conformation C_s–**8**–**su** (*A*–*B* 39.1°, *C*–*D* 55.8°) is less stable than C_s–**8**–**au** by 42.5 kJ/mol. It has very high pyramidalization of the carbons at the central double bond, $\chi(C^9)$ = 18.1°, $\chi(C^{9'})$ = –20.3°. These folded conformations are somewhat overcrowded: $C^{4'}\cdots C^{12'}$ and $C^{5'}\cdots C^{13'}$ distances are 303–304 pm (11% penetration), and $H^{4'}\cdots C^{12'}$ and $H^{5'}\cdots C^{13'}$ distances are ca. 258 pm (10% penetration). They also have a comparable degree of overcrowding in their *fjord* regions: the $C^1\cdots C^{1'}$ and $C^8\cdots C^{8'}$ distances in C_s–**8**–**au** and C_s–**8**–**su** are 307 and 313 pm (10 and 8% penetration), respectively, and the $H^1\cdots H^{1'}$ distance in C_s–**8**–**s** is 206 pm (11% penetration). The folded-twisted conformation [C_1–(*PP*)–**8**–**ft**] has moderately folded (*A*–*B* 10.2°) anthracenone which is rotated (ω_1 = 13.1°) relatively to the significantly folded (*C*–*D* 70.7°) dicyanomethylene substituted moiety. It serves as an "edge passage"[2b] transition state which connects the *anti*-folded and the *syn*-folded conformations of **8** with the enthalpy barriers of 88.2 and 45.7 kJ/mol, respectively. The shortest non-bonding distance $H^1\cdots C^{1'}$ in the *fjord* regions is 210 pm (27% penetration). The fourth folded conformation C_s–**8**–**f** (*A*–*B* 3.4°, *C*–*D* 74.7°) has nearly planar anthracenone moiety and no twisting. It is a second order saddle point due to even shorter, than in C_s–**7**–**f**, contacts in the *fjord* regions: $H^1\cdots C^{1'}$ and $H^8\cdots C^{8'}$ distances are 212 pm (26% penetration).

The twisted conformation C_1–(*MP*)–**8**–**tf** lies 42.3 kJ/mol higher than C_s–**8**–**au**. It demonstrates both the twisting (ω_1 = 55.3°, ω_2 = 1.1°) and the folding (*A*–*B* 7.8° in the anthracenone moiety, *C*–*D* 24.5° in the dicyanomethylene-substituted moiety) modes of deviation from coplanarity. It is more overcrowded than the folded conformations: the contact distances $C^{4'}\cdots C^{12'}$, $C^{5'}\cdots C^{13'}$, $H^{4'}\cdots C^{12'}$, and $H^{5'}\cdots C^{13'}$ are 288, 291, 238, and 243 pm (15–17% penetration). This conformation is chiral and undergoes enantiomerization through the pure twisted [C_2–(*MP*)–**8**–**tf**] transition state, with the barrier of ΔH_{298} = 16.4 kJ/mol. The enthalpy difference between C_1–(*MP*)–**8**–**tf** and C_s–**8**–**au** is significantly smaller than the enthalpy difference between the respective conformations of **7**: 42.3 vs. 61.3 kJ/mol. This is probably due to the contribution of the overcrowding caused by the dicyanomethylene groups at the *peri* H^4 and H^5 hydrogen atoms, which is enhanced in **7** (two dicyanomethylene groups) vs. **8** (one dicyanomethylene group). The enthalpy difference of 42.3 kJ/mol (the Gibbs free energy difference of 40.8 kJ/mol) between C_1–(*MP*)–**8**–**tf** and C_s–**8**–**au** prevents the twisted conformation from being thermally populated. Heteromerous BAE **8** can be classified as a Type 2 BAE and is not expected to exhibit a thermochromic behaviour, resembling BAE **7** rather then thermochromic BAE **2**.

Conclusions

BAEs **7** and **8** were found to be non thermochromic and belonging to Type 2 BAEs. The DFT study indicated that the avoidance of thermochromism by **7** and **8** is attributed to the decreased stabilities of their twisted conformations relative to the *anti*-folded conformations due to significant overcrowding caused by the presence of dicyanomethylene groups. The present study confirms that the threshold of 30 kJ/mol of enthalpy difference between twisted and *anti*-folded conformations can serve as a criterion of thermochromism.

Experimental Section

General: Melting points are uncorrected. All NMR spectra were recorded with a Bruker DRX 400 spectrometer. ^{1}H NMR spectra were recorded at 400.1 MHz using $CDCl_3$, $C_2D_2Cl_4$, CD_2Cl_2, and [D_6]DMSO, as solvents and as internal standards ($CHCl_3$, δ = 7.26 ppm), ($C_2H_2Cl_4$, δ = 5.99 ppm), (CH_2Cl_2, δ = 5.31 ppm), ([D_6]DMSO, δ = 2.60 ppm). ^{13}C NMR spectra were recorded at 100.6 MHz using $CDCl_3$, $C_2D_2Cl_4$ and CD_2Cl_2 as solvents and as internal standards ($CDCl_3$, δ = 77.01 ppm), ($C_2H_2Cl_4$, δ = 73.99 ppm), (CH_2Cl_2, δ = 53.37 ppm). Complete assignments were made through 2-dimensional correlation spectroscopy (DQF-COSY, HSQC, HMBC). UV/Vis spectra were measured using an

UVIKON 860 spectrometer. IR spectra were measured with a Perkin–Elmer System 2000 FT-IR spectrometer. Petroleum ether (PE, boiling range 40–60 °C) was used. X-ray data were collected on a Bruker SMART APEX CCD diffractometer equipped with a graphite monochromator and using Mo-K_α radiation (λ = 0.71073 Å) (Table 3).

Table 3. Crystallographic data for **7**.

	Low temperature	Room temperature
Empirical formula	$C_{34}H_{16}N_4$	$C_{34}H_{16}N_4$
Temperature [K]	173(1)	295(1)
Crystal system	monoclinic	monoclinic
Space group	$P2_1/n$	$P2_1/c$
a [Å]	16.1675(9)	8.1935(5)
b [Å]	8.8931(5)	8.9221(6)
c [Å]	16.6931(9)	16.759(1)
α [°]	90.0	90.0
β [°]	91.628(1)	91.733(1)
γ [°]	90.0	90.0
V [Å^3]	2399.2(2)	1224.6(1)
Z	4	2
Density (calcd.) [Mg m^{-3}]	1.330	1.303
Reflections collected	27344	14053
Independent reflections	5673	2896
Reflections observed	4699	2136
θ range [°]	1.73–28.01	2.43–28.00
R_{int}	0.0414	0.0451
R [$F^2 > 2\sigma(F^2)$]	0.0663	0.0427
wR [F^2]	0.1439	0.1025

[10-[10-(Dicyanomethylene)-9(10*H*)-anthracenylidene]-9(10*H*)-anthracenylidene]propanedinitrile (7) and [10-[10-Oxo-9(10*H*)-anthracenylidene]-9(10*H*)-anthracenylidene)]propanedinitrile (8): The reaction was carried out in a round-bottomed three-necked flask equipped with a reflux condenser protected from moisture and a magnetic stirrer. A stirred solution of bianthrone (**2**) (3.7 g, 9.6 mmol) and $CHCl_3$ (240 mL) was treated drop wise with $TiCl_4$ (4 mL, 36 mmol). The color of the solution turned black. The boiling reaction mixture was treated cautiously and rapidly with a solution of malononitrile (26.4 g, 0.4 mol, recrystallized from diethyl ether) and pyridine (65 mL, freshly distilled on KOH) in $CHCl_3$ (250 mL). The mixture was refluxed for 24 h. The reaction was monitored by TLC, until most of the starting material **2** had disappeared. To the cooled mixture chloroform (600 mL) was added. The solid residue was filtered off and extracted with boiling chloroform (500 mL). The volume of the combined chloroform filtrates was reduced to 200 mL by evaporation, and boiled for a few minutes. The resulting crude **7** (3.3 g, 14% yield) was filtered off. Recrystallization of 107 mg of **7** from boiling DMF (110 mL) gave 65 mg of **7**. Sublimation at 240 °C/0.1 mm for four days gave orange crystals, mp. ca. 466 °C (DSC curve). Evaporation of the filtrate to dryness gave **8** (0.3 g, 7.2% yield). The crude **8** was sublimed at 120 °C/0.1 mm for five days to give yellow-orange powder, m.p. 325 °C.

7: ^{1}H NMR (400 MHz, [D$_6$]DMSO, 298 K): δ = 7.238 (d, J = 7.8 Hz, H^1, H$^{1'}$, H^8, H$^{8'}$), 7.342 (t, J = 7.7 Hz, H^2, H$^{2'}$, H^7, H$^{7'}$), 7.514 (t, J = 7.7 Hz, H^3, H$^{3'}$, H^6, H$^{6'}$), 8.120 (d, J = 7.2 Hz, H^4, H$^{4'}$, H^5, H$^{5'}$) ppm. ^{1}H NMR (CD_2Cl_2, 298 K): δ = 7.212–7.257 (m, 4 H), 7.413–7.455 (m, 2 H), 8.092 (d, J = 7.8 Hz, 2 H) ppm. ^{1}H NMR ($C_2D_2Cl_4$, 348 K): δ = 7.247–7.309 (m, 4 H), 7.484 (t, J = 7.8 Hz, J = 1.5 Hz, 2 H), 8.146 (d, J = 7.8 Hz, 2 H) ppm. ^{13}C NMR ($C_2D_2Cl_4$, 348 K): δ = 99.70 ($C(CN)_2$), 113.90 (CN), 126.81 (CH), 128.49 (CH), 129.79 (CH), 130.32 (CH), 132.51 (C^9), 132.58 (C^{9a}), 135.39 (C^{4a}), 164.09 (C^{10}) ppm. UV/Vis (acetonitrile): c = 8.97×10^{-5} M): λ_{max} nm (ε): 417 (1060) 325 (1565) 283 (1435) 240 (1607) (ref.[2] 427 (13183) in DMSO, 423 (16596) in DMF). IR (KBr): $\tilde{\nu}_{max}$ = = 2219.5 (CN); 1576.4, 1547.2, 763.4, 695.5, 669.4 cm^{-1}. Calcd. for $C_{34}H_{16}N_4$: C 84.98, H 3.36, N 11.66; found C 84.94, H 3.22, N 11.64%. MS, 250 °C, m/z (%): 480 (100) [$C_{34}H_{16}N_4^+$], 452 (10) [$C_{34}H_{16}N_2^{+\cdot}$], 432 (23) [$C_{34}H_{10}N^{+\cdot}$], 416 (3) [$C_{31}H_{16}N_2^+$], 413 (12) [$C_{31}H_{15}N^{+\cdot}$], 240 (7) [$C_{17}H_8N_2^{+\cdot}$].

In an alternative workup of **8** the black filtrate was evaporated on silica gel and purified by column chromatography (silica gel 60, PE/EtOAc, gradient 0–30% of EtOAc). The first yellow fraction was collected. A second column chromatography (silica gel 60, PE/EtOAc, gradient 0–10% of EtOAc). The first fraction was collected. A yellow powder was obtained. It was identified as **8** free of traces of **2**: 0.015 g, yield 0.72%, and compared with an authentic sample of **8**.

8: ^{1}H NMR (400 MHz, $CDCl_3$, 298 K): δ = 7.087 (d, J = 8.0 Hz, 2 H), 7.146 (t, 2 H), 7.181 (d, 2 H), 7.232 (t, 2 H), 7.379 (t, 2 H), 7.450 (t, 2 H), 8.074 (d, 2 H), 8.145 (d, 2 H) ppm. ^{1}H NMR ($C_2D_2Cl_4$, 298 K): δ = 7.098 (d, J = 7.7 Hz, 2 H), 7.164–7.211 (m, 4 H), 7.275 (t, J = 7.7 Hz, 2 H), 7.412 (t, J = 7.7 Hz, 2 H), 7.472 (t, J = 7.2 Hz, 2 H), 8.056 (d, J = 8.0 Hz, 2 H), 8.126 (d, J = 7.7 Hz, 2 H) ppm. ^{13}C NMR ($CDCl_3$, 298 K): δ = 113.84, 126.66 (CH), 127.03 (CH), 128.08 (CH), 128.78 (CH), 129.68 (CH), 129.72 (CH), 129.87 (CH), 130.39 (CH), 132.13, 132.33, 132.89, 134.04, 136.23, 138.11, 164.63, 186.24 (CO) ppm. ^{13}C NMR ($C_2D_2Cl_4$, 298 K): δ = 79.18 ($C(CN)_2$), 114.15 (CN), 126.65 (CH), 127.02 (CH), 128.25 (CH), 129.00 (CH), 129.81 (CH), 129.85 (CH), 130.15 (CH), 130.63 (CH), 132.23 (C), 132.34(C), 132.75(C), 133.88(C), 136.14 (C), 138.11 (C), 164.87 (C$^{10'}$), 186.33 (C^{10}) ppm. UV/Vis (acetonitrile): c = 7.94×10^{-5} M): λ_{max} nm (ε): 390 (570), 330 (695), 305 (880) (sh), 264 (1890), 240 (21054). IR (KBr): $\tilde{\nu}_{max}$ = 2222.3 (CN), 1671.8 (CO), 1301.7, 1275.7, 1163.2, 928.7, 768.0, 734.5, 701.1 cm^{-1}. $C_{31}H_{16}N_2O$: C 86.09, H 3.73, N 6.48; found C 86.10, H 3.98, N 5.49%. MS, 190 °C, m/z (%): 433 (34) [$^{13}CC_{30}H_{16}N_2O^+$], 432 (100) [$C_{31}H_{16}N_2O^+$], 385 (27) [$C_{31}H_{13}^+$], 384 (83) [$C_{31}H_{12}^{\cdot+}$], 355 (29) [$C_{27}H_{15}O^+$].

Computation Details: The quantum mechanical calculations of the BAEs under study were performed with the Gaussian03[24] package. Becke's three parameter hybrid density functional B3LYP,[25] with the non-local correlation functional of Lee, Yang, and Parr[26] was used. The basis sets STO-3G, 6-31G(d) and 6-311G(d,p) were employed. All structures were fully optimized, using symmetry constrains as indicated. Vibrational frequencies were calculated to verify the nature of the stationary points at B3LYP/6-31G(d) and at B3LYP/6-311G(d,p). Non-scaled thermal corrections to enthalpy and to free energy calculated at the specified levels were applied. Intrinsic Reaction Coordinate calculations at B3LYP/STO-3G and B3LYP/6-31G(d) were used to identify the minima connected through the transition states.

Supporting Information (see also the footnote on the first page of this article): DFT total energies and Z-matrices of **7** and **8**.

[1] C. de la Harpe, W. A. van Dorp, *Ber. Dtsch. Chem. Ges.* **1875**, *8*, 1048–1050.

[2] a) G. Shoham, S. Cohen, R. M. Suissa, I. Agranat, in *Molecular Structure: Chemical Reactivity and Biological Activity* (Eds.: J. J. Stezowski, J.-L. Huang, M.-C. Shao), IUCr Crystallographic Symposia 2, Oxford University Press, Oxford, **1988**, pp. 290–312; b) P. U. Biedermann, J. J. Stezowski, I. Agranat, in *Advances in Theoretically Interesting Molecules* (Ed.: R. P. Thummel), vol. 4, JAI Press, Stanford, CN, **1988**, pp. 245–322; c) P. U. Biedermann, J. J. Stezowski, I. Agranat, *Eur. J. Org. Chem.* **2001**, 15–34.

[3] a) E. D. Bergmann, *Prog. Org. Chem.* **1955**, *3*, 81–171; b) J. H. Day, *Chem. Rev.* **1963**, *63*, 65–80; c) G. Kortüm, *Ber. Bunsen-Ges. Phys. Chem.* **1974**, *78*, 391–403; d) A. Samat, V. Lokshin, in *Organic Photochromic and Thermochromic Compounds* (Eds.: J. C. Crano, R. J. Guglielmetti), vol. 2, Plenum Press, New York, **1999**, p. 415; e) H. Bouas-Laurent, H. Dürr, *Pure Appl. Chem.* **2001**, *73*, 639–665; f) P. U. Biedermann, J. J. Stezowski, I. Agranat, *Chem. Eur. J.* **2006**, *12*, 3345–3354.

[4] a) H. Meyer, *Ber. Dtsch. Chem. Ges.* **1909**, *42*, 143–145; b) H. Meyer, *Monatsh. Chem.* **1909**, *30*, 165–177.

[5] D. L. Fanselow, H. G. Drickamer, *J. Chem. Phys.* **1974**, *61*, 4567–4574.

[6] a) Y. Hirshberg, *Compt. Rend.* **1950**, *231*, 903–904; b) G. Kortüm, W. Theilacker, V. Braun, *Z. Physik. Chem.* **1954**, *NF 2*, 179–196; c) T. Bercovici, R. Korenstein, K. A. Muszkat, E. Fischer, *Pure Appl. Chem.* **1970**, *24*, 531–565; d) E. Fischer, *Chem. Unserer Zeit* **1975**, *9*, 85–95; e) E. Fischer, *Rev. Chem. Intermed.* **1984**, *5*, 393–422; f) K. A. Muszkat in *The Chemistry of Quinonoid Compounds* (Eds.: S. Patai, Z. Rappoport), vol. 2, Wiley, Chichester, **1988**, pp. 203–224; g) W. H. Laarhoven in *Photochromism, Molecules and Systems* (Eds.: H. Dürr, H. Bouas-Laurent), Elsevier, Amsterdam, **1990**, pp. 270–313; h) *Organic Photochromic and Thermochromic Compounds* (Eds.: J. C. Crano, R. J. Guglielmetti), *Topics in Applied Chemistry*, vol. 1, *Photochromic Families*, vol. 2, *Physicochemical Studies, Biological Applications, and Thermochromism*, Plenum Press, New York, **1999**.

[7] B. L. Feringa, *Acc. Chem. Res.* **2001**, *34*, 504–513.

[8] a) K. Linde, G. Ramirez, C. D. Mulrow, A. Pauls, W. Weidenhammer, D. Melchart, *Brit. Med. J.* **1996**, *313*, 253–258; b) M. Philipp, R. Kohnen, K.-O. Hiller, K. Linde, M. Berner, *Brit. Med. J.* **1999**, *319*, 1534–1539.

[9] R. Herges, *Chem. Rev.* **2006**, *106*, 4820–4842.

[10] a) W. T. Grubb, G. B. Kistiakowsky, *J. Am. Chem. Soc.* **1950**, *72*, 419–424; b) W. Theilacker, G. Kortüm, G. Friedheim, *Ber. Dtsch. Chem. Ges.* **1950**, *83*, 508–519; c) Y. Hirschberg, E. Fischer, *J. Chem. Soc.* **1953**, 629–636; d) G. Kortüm, *Angew. Chem.* **1958**, *70*, 14–20; e) Z. R. Grabowski, M. S. Balasiewicz, *Trans. Faraday Soc.* **1968**, *64*, 3346–3353; f) Y. Tapuhi, O. Kalisky, I. Agranat, *J. Org. Chem.* **1979**, *44*, 1949–1952; g) T. Natsue, D. H. Evans, *J. Electroanal. Chem.* **1984**, *168*, 287–298.

[11] a) E. Harnik, *J. Chem. Phys.* **1956**, *24*, 297–299; b) E. Wasserman, R. E. Davis, *J. Chem. Phys.* **1959**, *30*, 1367; c) G. Kortüm, G. Bayer, *Ber. Bunsen-Ges. Phys. Chem.* **1963**, *67*, 24–28; d) R. Korenstein, K. A. Muszkat, E. Fischer, *Helv. Chim. Acta* **1970**, *53*, 2102–2109.

[12] P. U. Biedermann, J. J. Stezowski, I. Agranat, *Chem. Commun.* **2001**, 954–955.

[13] The photochemical conversion of *anti*-folded **4** to *syn*-folded conformer at low temperature anr the thermal reversion of the latter to the *anti*-folded **4** have recently been reported: W. R. Browne, M. M. Pollard, B. de Lange, A. Meetsma, B. L. Feringa, *J. Am. Chem. Soc.* **2006**, *128*, 12412–12413.

[14] A. Levy, P. U. Biedermann, I. Agranat, *Org. Lett.* **2000**, *2*, 1811–1814.

[15] A. Levy, S. Pogodin, S. Cohen, I. Agranat, *Eur. J. Org. Chem.* **2007**, 5198–5211.

[16] A. Aumüller, S. Hünig, *Lieb. Ann. Chem.* **1984**, 618–621.

[17] S. Yamaguchi, T. Hanafusa, T. Tanaka, M. Sawada, K. Kondo, M. Irie, H. Tatemitsu, Y. Sakata, S. Misumi, *Tetrahedron Lett.* **1986**, *27*, 2411–2414.

[18] A. M. Kini, D. O. Cowan, F. Gerson, R. Möckel, *J. Am. Chem. Soc.* **1985**, *107*, 556–562.

[19] I. Agranat, Y. Tapuhi, *J. Org. Chem.* **1979**, *44*, 1941–1948.

[20] CCDC-665680 (for **RT-7**) and -665681 (for **LT-7**) contain the supplementary crystallographic data for this paper. These data can be obtained free of charge from The Cambridge Crystallographic Data Centre via www.ccdc.cam.ac.uk/data_request/cif.

[21] Yu. V. Zefirov, *Crystallogr. Rep. (Kristallografiya)* **1997**, *42*, 111–116.

[22] a) F. De Proft, P. Geerling, *Chem. Rev.* **2001**, *101*, 1451–1464; b) W. Koch, M. C. Holthausen, *A Chemist Guide to Density Functional Theory*, Wiley-VCH, Weinheim, **2000**.

[23] S. Pogodin, I. D. Rae, I. Agranat, *Eur. J. Org. Chem.* **2006**, 5059–5068.

[24] M. J. Frisch, G. W. Trucks, H. B. Schlegel, G. E. Scuseria, M. A. Robb, J. R. Cheeseman, J. A. Montgomery Jr, T. Vreven, K. N. Kudin, J. C. Burant, J. M. Millam, S. S. Iyengar, J. Tomasi, V. Barone, B. Mennucci, M. Cossi, G. Scalmani, N. Rega, G. A. Petersson, H. Nakatsuji, M. Hada, M. Ehara, K. Toyota, R. Fukuda, J. Hasegawa, M. Ishida, T. Nakajima, Y. Honda, O. Kitao, H. Nakai, M. Klene, X. Li, J. E. Knox, H. P. Hratchian, J. B. Cross, C. Adamo, J. Jaramillo, R. Gomperts, R. E. Stratmann, O. Yazyev, A. J. Austin, R. Cammi, C. Pomelli, J. W. Ochterski, P. Y. Ayala, K. Morokuma, G. A. Voth, P. Salvador, J. J. Dannenberg, V. G. Zakrzewski, S. Dapprich, A. D. Daniels, M. C. Strain, O. Farkas, D. K. Malick, A. D. Rabuck, K. Raghavachari, J. B. Foresman, J. V. Ortiz, Q. Cui, A. G. Baboul, S. Clifford, J. Cioslowski, B. B. Stefanov, G. Liu, A. Liashenko, P. Piskorz, I. Komaromi, R. L. Martin, D. J. Fox, T. Keith, M. A. Al-Laham, C. Y. Peng, A. Nanayakkara, M. Challacombe, P. M. W. Gill, B. Johnson, W. Chen, M. W. Wong, C. Gonzalez, J. A. Pople, *Gaussian 03*, Revision C.02, Gaussian, Inc., Wallingford CT, **2004**.

[25] A. D. Becke, *J. Chem. Phys.* **1993**, *98*, 5648–5652.

[26] C. Lee, W. Yang, R. G. Parr, *Phys. Rev. B* **1988**, *37*, 785–789.

Received: November 28, 2007
Published Online: April 25, 2008

